Water Level Prediction of Emergency Groundwater Source and Its Impact on the Surrounding Environment in Nantong City, China

Jinbang Cai [1], Ping Wang [2], Huan Shen [2,*], Yue Su [2] and Yong Huang [2]

[1] Nanjing Institute of Environmental Sciences, Ministry of Ecology and Environment, Nanjing 210042, China; cjb@nies.org

[2] School of Earth Science and Engineering, Hohai University, Nanjing 210098, China; pingwang@hhu.edu.cn (P.W.); suyue@hhu.edu.cn (Y.S.); hyong@hhu.edu.cn (Y.H.)

[*] Correspondence: shenh@hhu.edu.cn; Tel.: +86-1529-575-7958

check for updates

Abstract: Based on the geological and hydrogeological conditions, and in situ hydrogeological tests of the emergency groundwater source in Nantong City, China, a 3D numerical model of the heterogeneous anisotropy in the study area was established and calibrated using data from pumping and recovery tests. The calibrated model was used to simulate and predict the water level of the depression cone during the emergency pumping and water level recovery. The results showed that after seven days of pumping, the water level in the center of the depression cone ranged from −51 m to −55 m, and compared with the initial water level, the water level dropped by 29 m to 32 m. The calculated water level has a small deviation compared with that of the analytical solution, which indicates the reliability and rationality of the numerical solution. Furthermore, during water level recovery, the water level of pumping wells and its surroundings rose rapidly, which was a difference of about 0.28 m from the initial water level after 30 days, indicating that the groundwater level had recovered to the state before pumping. Due to the emergency pumping time is not long, the water levels of Tonglu Canal, surrounding residential wells, and other aquifers will not be affected. After stopping pumping, the water level recovers quickly, so the change of water level in a short time will not lead to large land subsidence and has little impact on the surrounding environment.

Keywords: emergency groundwater source; numerical model; drawdown; in situ hydrogeological tests

1. Introduction

With the rapid economic development and the acceleration of urbanization, large-scale water pollution in cities has occurred from time to time in recent years, such as the Songhua River, Taihu Lake and Beijiang River and other surface water pollution incidents. The safety of urban water supply is seriously threatened [1–4]. Because the groundwater is less vulnerable to be polluted, it has become an important part of the urban water supply source [5,6]. The emergency water source, as a temporary water supply source that guarantees the basic living water of residents, plays an important role in dealing with large-scale water shortages or water pollution in cities that cause water supply difficulties [7–9].

As many sudden water safety issues are frequently discovered, humans' awareness of prevention of secondary drinking water crises has also been continuously improved. For many countries and regions, the emergency water source has become an important part of the safety guarantee system and the construction of strategic emergency water source has also become an urgent problem to be solved [10–14].

International experts and researchers have done a lot of theoretical and applied research work on the development and utilization of groundwater emergency water source so far [15–23]. Praveen Kumar Amar [24] proposed that water resources in emergency water sources need to be dynamically adjusted and allocated reasonably. Lan et al. [25] established a groundwater flow and migration model based on regional hydrogeological conditions and monitoring data from 52 boreholes, and then carried out water level prediction and environmental impact assessment on the withdrawal plan of the emergency groundwater source in Jiujiang City along the Yangtze River. The results showed that short-term emergency water supply had little impact on the environment. According to the characteristics of emergency water supply, Dai et al. [26] divided water sources into emergency water sources and backup water sources. Taking a northern city in China as an example, a systematic study was conducted on the factors affecting groundwater sources and the environmental effects caused by emergency withdrawal. Zhu et al. [27] established a migration model for the Dawu water source through MODFLOW, which was used to simulate and predict the migration of pollutants in the water source under the action of water interception wells and extraction wells. Song et al. [28] gave a detailed overview of the optimal allocation of urban water supply from the perspectives of changes, modeling methods and challenges and it provided a reference for the construction of urban groundwater sources. In order to identify the influencing factors and environmental impacts of reservoir-type water sources, the reservoir-type water source vulnerability (WSV) assessment method was established by Zhang et al. and was successfully applied to Tianjin Yuqiao Reservoir [29]. In order to evaluate the feasibility of using groundwater as an emergency water source to alleviate the effects of drought, the groundwater model in arid areas was established by Mussá et al. [30] In order to use limited groundwater resources more efficiently and rationally, Bozek et al. [31] proposed a semi-quantitative risk assessment method for emergency groundwater source to improve the distribution and dispatch of groundwater resources in the Czech Republic. Capelli et al. [32] discussed an approach for identifying "strategic groundwater resources" for human consumption and the approach was illustrated in the northern Latium volcanic complexes of Italy. Perfler et al. [33] studied and analyzed the factors affecting the safety and quality of drinking water in Austria, and put forward detailed requirements. In order to better respond to urban emergencies, Zhang et al. [34] analyzed the feasibility of karst groundwater as an emergency groundwater source from the perspective of environmental geology. They believed that the emergency withdrawal will not cause problems such as ground collapse and water pollution. Guo et al. [35] analyzed and studied the groundwater dynamics and flow field evolution characteristics of Huairou emergency water source during the recent 30 years of withdrawal. Wu et al. [36] built a regional groundwater numerical model. The groundwater level recovery capacity of the emergency groundwater source area in Ningbo was predicted under the condition of emergency withdrawal and the environmental effects of groundwater fall funnel, ground subsidence and salt water intrusion caused by emergency withdrawal were evaluated. Ye et al. [37] discussed the concept, characteristics and selection of emergency water source and they also demonstrated the feasibility of constructing emergency water sources in Xinchengzi District of Shenyang. Based on the current water demand and groundwater characteristics of Jilin City in China, Liu et al. [38] carried out a systematic modeling of groundwater emergency source determination, emergency capability analysis and emergency withdrawal plan design. The prediction results of the model showed that the drawdown of the five emergency withdrawal schemes (30 days, 60 days, 90 days, 180 days, and 360 days) was 2.0–8.0 m, which had little impact on the overall groundwater level of Jilin City and the environmental risk was little.

In summary, most of the existing research on emergency groundwater source mainly focuses on the qualitative analysis of emergency water source locations, dynamic characteristics, plan optimization, and protection countermeasures [39–43]. Only a few researchers have explored the environmental impact of groundwater exploitation. The research on water level prediction and environmental impact during the operation period of the groundwater emergency source area is not enough [44–46]. Taking the emergency groundwater source in Nantong as an example, the purpose of this paper is to predict the

dynamic changes of the groundwater level and evaluate the impact on the surrounding environment. Firstly, the general situation, topographic features, stratum situation and hydrogeological conditions of the emergency groundwater source in Nantong are described. Then, the numerical method and model calibration method are introduced. Finally, the groundwater level during pumping and recovery is predicted and the impact of the emergency groundwater source on the surrounding environment is analyzed in detail from multiple perspectives based on the situation of the project area, which provides some references for the construction and operation of emergency groundwater source.

2. Study Site

2.1. Study Area

The emergency groundwater source of Nantong is located in Limin Village, Tongzhou District, Jiangsu Province, the length is 801.77 m, the width is 190.1 m, and the total area is 138,115 m^2. The project involves thirteen pumping wells, of which two wells are test wells J_1 and J_2. Groundwater pumping volume for a single well is 1920 m^3/day, and the total pumping volume is 25,000 m^3/day. There are seven wells on the side close to the Tonglu Canal, with a distance of 127–130 m between the wells. The other six wells are on the side far from the riverbank, with a distance of 134–148 m between the wells. The annual average temperature in this area is 15.1 °C, and that of January and July are 2.5 and 27.3 °C, respectively. The annual average precipitation and evaporation are 1084 mm and 857 mm, respectively. The spatial and temporal distribution of precipitation is uneven and mainly concentrated in the summer and autumn. Among them, the plum rain and typhoon rain are mainly from June to July, August to September, respectively. The location of study area and pumping wells is shown in Figure 1.
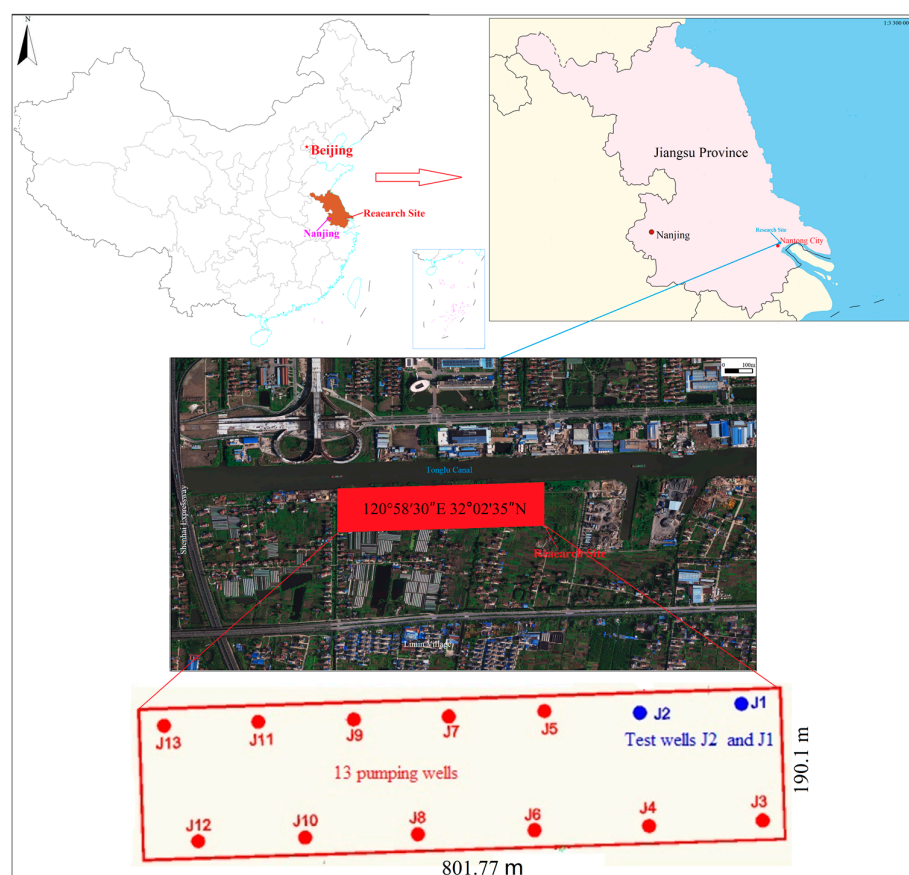

Figure 1. Location of study area and pumping wells.

2.2. Topographic Features

The terrain of Nantong is flat, and the ground elevation is about between 3.2 m and 4.5 m over the sea level. The northwest area is slightly higher than in the southeast. The landforms mainly include three plain areas, namely, (1) delta plain: it is the area extending outward from the ancient barrier spit on the north bank of the Yangtze River. It is also the area where the estuary sandbank contacted the land in the early stage. This landform belongs to the range of fluvial marine deposits and starts from north Fangong dike in the south to Changsha town in the west. There are dish-shaped pits in some areas, such as Zhanghuangdang, Changshadang, and so on; that is, the elevation is less than 3 m. Since the soil in this area was formed earlier, it developed into fluvo-aquic soil after artificial, dry plowing, and maturation; (2) water net plain: this area is distributed in the middle, centered on the sediment zone of ancient river branch in Nantong, extending south to Tonglu Canal sediment zone. The eastern area is higher, with an elevation of about 5 m. The water network here is dense and mostly composed of river and lake silt. The water net polder plain is located in the northern part of Haian and is a low-lying plain area in the Lixia River lagoon sediment zone. The elevation is below 4 m, the farming conditions are better, and the soil fertility is high; and (3) marine deposition plain: the eastern estuary of the mainstream of the Yangtze River, the ancient Hengjiang River, namely the marine deposition plain. The main terrain trend of this area is that the levee on both sides is titled toward the center. Nowadays, the marine sediments outside Fangong dike are mostly artificially modified soils that have formed fluvo-aquic saline soil. The salt content in the 1 m soil is also low at 0.6%, the groundwater salinity ranges from 3.0 to 5.0 g/L, and part of the soil is transitioning to fluvo-aquic soil. The topographic map of the study area is shown in Figure 2.
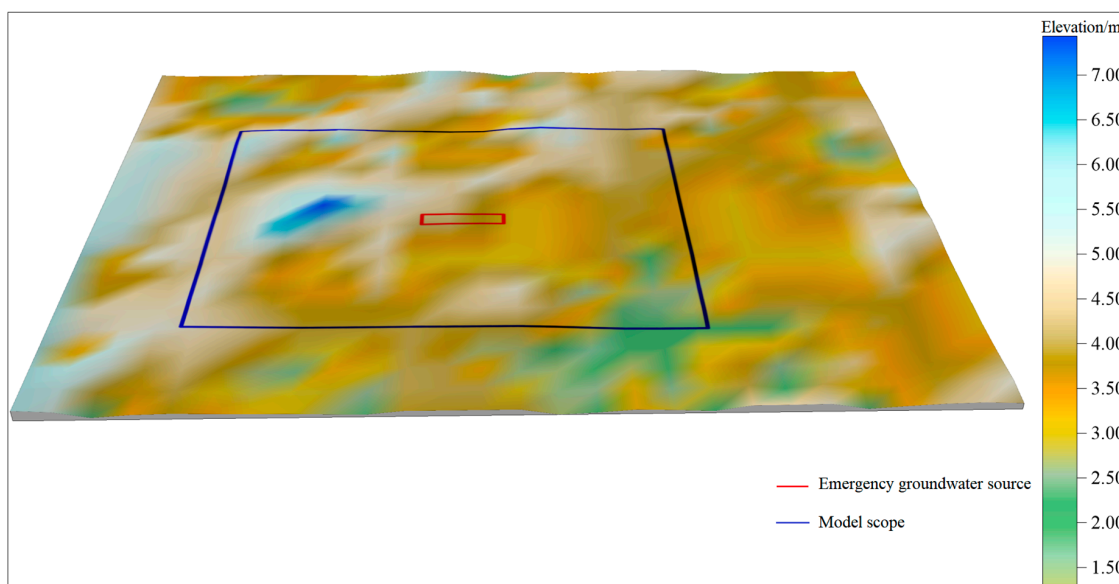

Figure 2. Topographic map of the study area.

2.3. Geological Setting

The area is mainly overlain by Quaternary alluvial deposits which consist of loose sediments with rhythmic changes alternately appearing in sand and clay layers [47]. The thickness of the Quaternary aquifer ranges from 240 m to 300 m. The sedimentary sequence is complex and phase changes are frequent. According to the difference of sedimentary sequence, the Quaternary system can be divided into Lower, Middle, and Upper Pleistocene and Holocene deposits. (1) Lower Pleistocene Series: The overall sequence is a set of fluvial sequences, and the middle section is affected by transgression in some areas and shows the characteristics of estuary sedimentation. The complete basic sequence consists of gravel-bearing coarse sand and medium-fine sand at the bottom, and transitions upward to

silty sand and clay loam, showing a complete fluvial facies dual-texture. The thickness of the strata is between 100 m and 150 m. (2) Middle Pleistocene Series: The lithology is divided into upper and lower sections. The lower section is mainly silty sand, fine sand, medium-coarse sand, and gravel-bearing medium-coarse sand, and the upper section is mainly silty clay, silty sand, and fine sand. The thickness of the strata is between 30 m and 60 m. (3) Upper Pleistocene Series: The lithological characteristics are mainly gray, gray-green silty-fine sand. The sedimentary environment is dominated by fluvial facies, and later it appears as floodplain facies. The thickness of the strata is about 100 m. (4) Holocene Series: It is composed of delta facies deposits consist of gray silt and gray-black mucky clay, and a combination of fine clastics mainly composed of silty sand, sandy loam and mucky clay. The thickness of the strata is between 15 m and 50 m.

2.4. Hydrogeological Conditions

(1)   Aquifer types

According to the nature of aquifers and the prospecting data, the aquifers are divided into four categories: the phreatic aquifer, the first confined aquifer, the second confined aquifer, and the third confined aquifer [48]. The hydrogeological map of the study area is shown in Figure 3.

a.   The phreatic aquifer

The aquifer formation is composed of Holocene Series (Q_4) Yangtze River delta facies which consist of silty clay, silty sand, and silty-fine sand. The buried depth is above 50 m. In the vertical section, the mineral particles in the upper and lower sections are coarser, while in the intermediate section, the mineral particles become finer. The area is divided into two water-bearing sections, namely, the upper and lower water-bearing sections. The upper section is suitable for residential wells, with a small depth, mainly used for washing and irrigation of residents. The lower section is more suitable for shallow wells, with a depth of about 20 m, mainly used for water source extraction in phreatic aquifers during dry periods. The burial depth of the water level fluctuates up and down with the change of seasons, and the water level varies within the range of 1 to 3 m. The lower aquifer has a nature of semiconfined aquifer, and certain sections are connected to the first confined water. The quantity of groundwater pumped of a single well in the upper water-bearing section is not less than 10 m^3/day and the lower above 100 m^3/day. The water quality is freshwater-brackish water, with a salinity of 1 to 1.5 g/L. Due to the low quantity of groundwater pumped, poor water quality, and lack of stability, there is currently no large-scale exploitation in the area. The dynamic variation of groundwater level in the phreatic and the first confined aquifer are shown in Figure 4.
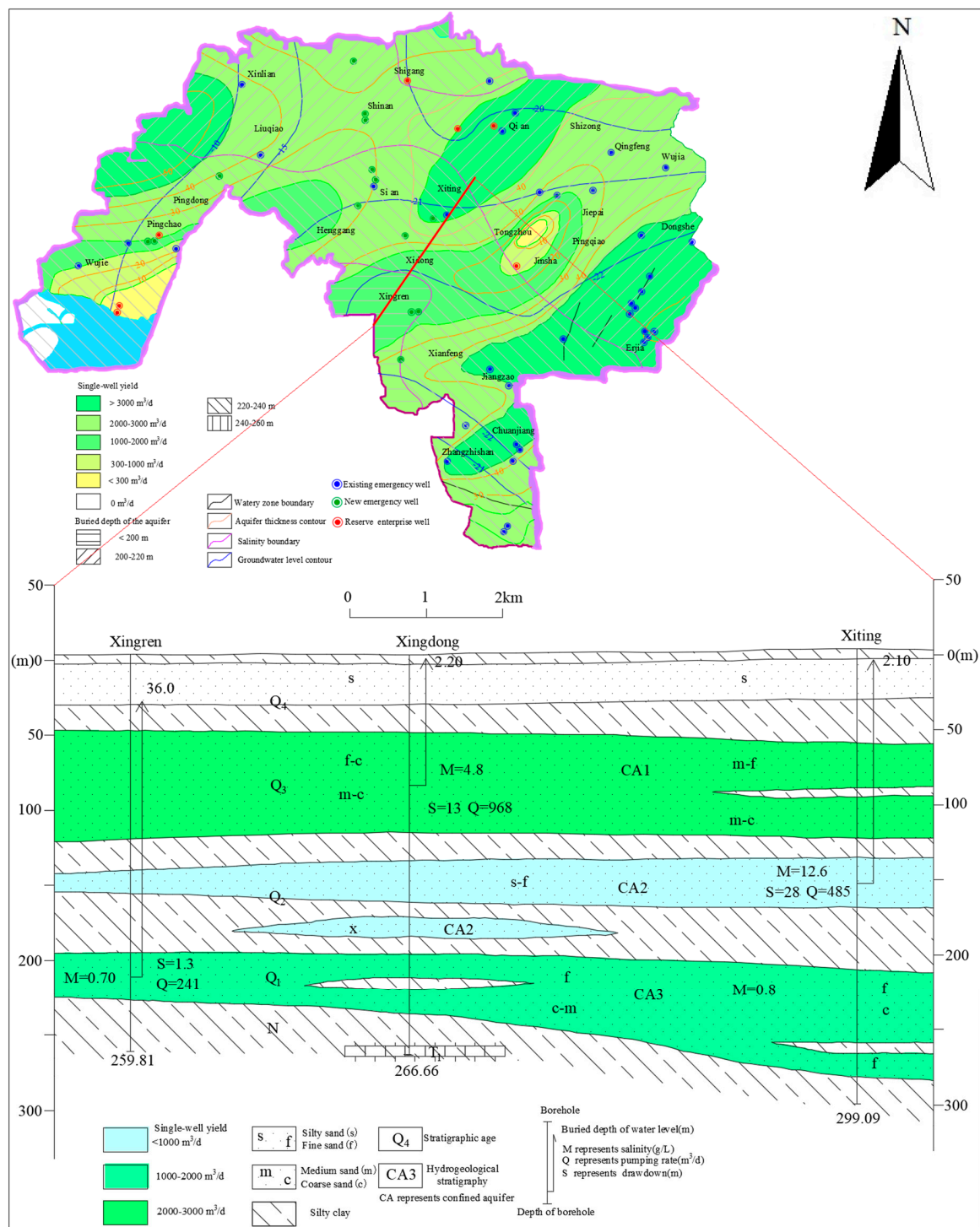
Figure 3. Hydrogeological map of the study area.

b.　The first confined aquifer

The first confined aquifer is mainly composed of the Upper Pleistocene alluvial and alluvial-marine loose sand layer, and the secondary transgression has had a great impact on it. The burial depth of the upper interface of the aquifer ranges from 50 m to 60 m. The lithology is mainly mucky clay or silty clay, and there is silty sand inter-bedded silt in some local areas. The thickness of the aquifer ranges from 10 m to 20 m. The impervious layer composed of gray-yellow, brown-yellow silty clay, clay, and mucky soil forms the lower interface of the aquifer formation. The aquifer in this area is composed

of sand pebbles, gravel layers, gravel-bearing coarse sand, medium-coarse sand, medium-fine sand, fine sand, silty sand. The thickness of the aquifer is more than 60 m. The elevation of water level in the first confined aquifer is between 0 and 2 m, but the groundwater level may have dropped to the lowest value of −0.84 m due to the increase in artificial exploitation around in July 2013 (Figure 4). This aquifer is highly permeable and has abundant recharge sources. The discharge rate of a single well is usually between 2000 and 3000 m^3/day. The water quality is relatively poor and is brackish water with a salinity of more than 3.0 to 5.0 g/L.
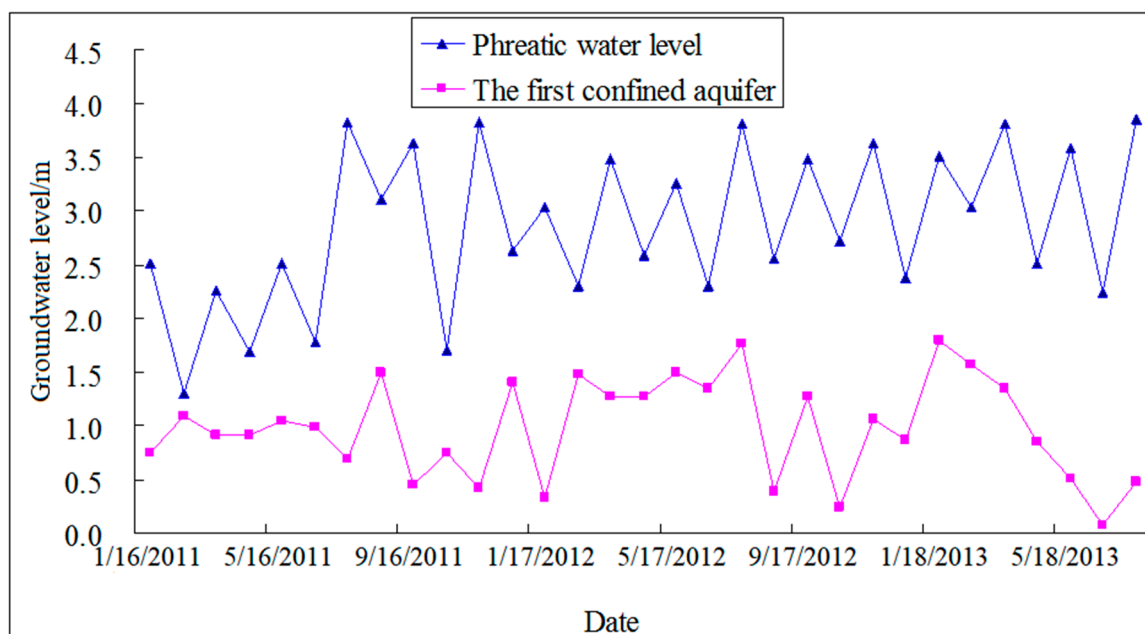

Figure 4. Dynamic variation of groundwater level.

c. The second confined aquifer

The second confined aquifer is composed of blanket sand formed near the estuary of the Yangtze River during the Middle Pleistocene. The buried depth of the upper interface of the aquifer ranges from 130 m to 150 m. The lithology is mainly gravel-bearing fine and medium-coarse sand, which turns into silty sand in the upper part. The thickness of the aquifer ranges from 25 to 30 m. The quantity of groundwater pumped of a single well is 1000 m^3/day, and the buried depth of static level is in the range of 3 m to 5 m. The salinity is more than 1.0 g/L. At this stage, there is no exploitation activity. The dynamic variation of groundwater level in the second confined aquifer is shown in Figure 5.

d. The third confined aquifer

The depositional age of the third confined aquifer is the Lower Pleistocene Series (Q_1). The buried depth of the upper interface of the aquifer is 200 m. The lithology is gravel-bearing fine and medium-coarse sand. The thickness of the aquifer ranges from 20 to 25 m. This aquifer is the main exploitation horizon due to its better water richness, wide distribution, and guaranteed water quality. The lithology is mainly gravel-bearing medium-coarse sand, coarse sand, fine sand or gravel-bearing coarse sand, medium-fine sand, silty sand. The quantity of groundwater pumped from the single well ranges from 1000 and 2000 m^3/day. Because the third confined aquifer has good burial conditions, the clay loam of the upper interface is dense and brown, with a relatively stable distribution, and a large thickness, effectively blocking the saltwater from the upper first confined aquifer and second confined aquifer. Therefore, the water quality of the confined aquifer in this area is better than that of other aquifers and is suitable for residents, with salinity less than 1.0 g/L and hardness less than 50 mg/L. The water type is mainly freshwater type, and the water temperature ranges from generally

22 to 23 °C. Due to the deep burial, it is relatively difficult to recharge the groundwater and to fully recover to the static level in a short time. Therefore, the water level fluctuates greatly and water level elevation ranges from −22 to −30 m. The water level change is mainly caused by artificial exploitation. The dynamic variation of groundwater level in the third confined aquifer is shown in Figure 6.
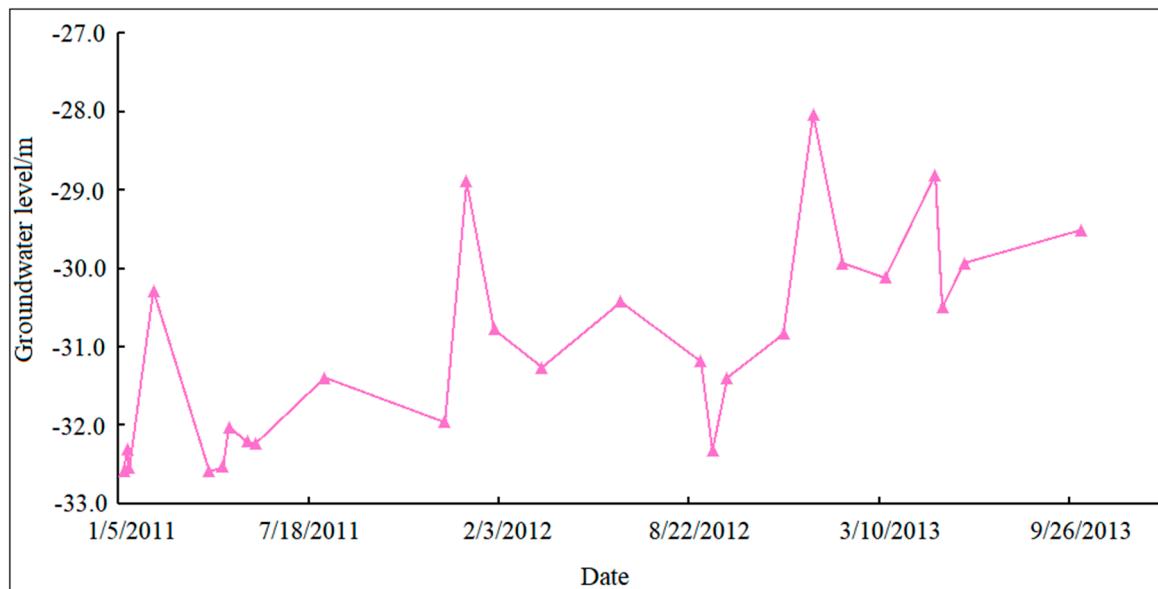

Figure 5. Dynamic variation of groundwater level in the second confined aquifer.

(2)   Recharge, runoff, and discharge of groundwater

The phreatic aquifer is closely related to surface water due to its small buried depth and distributes a wide range, and there is a complementary relationship between them. The aquifer is recharged by atmospheric precipitation infiltration, lateral infiltration of surface water bodies, and return of farmland irrigation water. Since this area is located in the estuary area of the Yangtze River delta, the lithological particles of the phreatic aquifer are relatively coarse and the permeability is relatively high, so the runoff conditions are relatively good. The aquifer is discharged by vertical and horizontal direction from phreatic water evaporation, lateral infiltration of surface water bodies and leakage recharge to deep aquifers, and artificial exploitation. Among them, artificial exploitation and phreatic evaporation are the main discharge pathways.

The phreatic aquifer is recharged by atmospheric precipitation infiltration, and then recharged to the first confined aquifer by the leakage, so there is a certain hydraulic connection between the first confined aquifer and phreatic aquifer in this area. Between the first confined aquifer and second confined aquifer, the thickness of the impermeable layer in some sections is very small, only 5–15 m. Therefore, the two aquifers have a relatively close hydraulic connection and a complementary relationship. This area is located downstream of the regional seepage field. The regional seepage recharge comes from the upstream of the northwest and is mainly recharged by atmospheric precipitation infiltration. The confined water-bearing sand layer has high water permeability. Under the effect of hydraulic head, the groundwater produces regional runoff from west to east, which makes the confined water recharge laterally. The runoff and discharge of the first confined aquifer and second confined aquifer are mainly restricted by two factors: regional circulation and artificial exploitation. The former is mainly controlled by the groundwater flow field in the Yangtze River delta and the seepage velocity depends on the hydraulic gradient of the groundwater. Generally speaking, it flows from west to east and from north to south slowly, and the discharge direction is from upstream to downstream. Secondly, artificial exploitation and leakage recharge are also one of the ways of runoff and discharge.
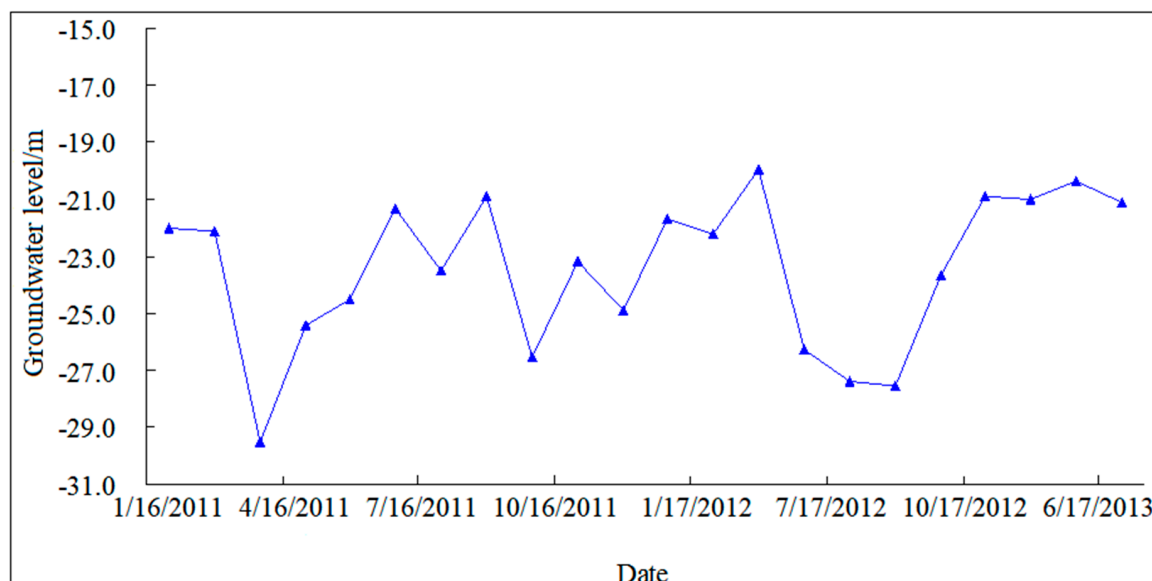
Figure 6. Dynamic variation of groundwater level in the third confined aquifer.

Recharge sources of the third confined aquifer are from the upstream recharge area, lateral recharge of the aquifer in the adjacent area and the elastic and plastic storage of the aquifer. The third confined water runoff in this area mainly flows from north to south, namely from the weak exploitation area to the strong exploitation area. As of the end of 2012, the number of third confined water extraction wells in this area was 105, most of which were located in the southern region, accounting for about 70% of the total. Land subsidence had already occurred in some areas due to overexploitation of groundwater. From north to south, the groundwater level gradually dropped from −15 m to −30 m. The main way of discharge in the third confined water was artificial exploitation.

3. Methods

3.1. Numerical Method

In this study area, numerical methods were used to simulate the groundwater flow movement by using the FEFLOW software (Finite Element Subsurface Flow System). It is developed by Wasy GmbH, Institute for Water Resources Planning and Systems Research Ltd. Germany [49]. It can simulate the regional seepage field and the planning and management plan of groundwater resources, and simulate the impact of underground exploitation on regional groundwater and its optimal countermeasures. It combines the precipitation-runoff model to dynamically simulate the "precipitation-surface water-groundwater" water resources system, analyzes the interdependence between the various components of the water resources system, and studies the rational use of water resources and the impact of ecological environment protection. In this study, the software is used to simulate the change of groundwater level in the third confined aquifer under pumping conditions. The numerical results can provide a relevant basis for the operation of emergency groundwater sources.

Based on the hydrogeological conditions of the study area, a mathematical model of the three-dimensional groundwater flow movement in the study area can be expressed as [50,51]:

$$
\begin{cases}
\frac{\partial}{\partial x}\left(K_{xx}\frac{\partial H}{\partial x}\right) + \frac{\partial}{\partial y}\left(K_{yy}\frac{\partial H}{\partial y}\right) + \frac{\partial}{\partial z}\left(K_{zz}\frac{\partial H}{\partial z}\right) + W = S_s\frac{\partial H}{\partial t} & (x,y,z) \in \Omega \\[4pt]
H(x,y,z,t)\big|_{t=0} = H(x,y,z,t_0) & (x,y,z) \in \Omega \\[4pt]
H(x,y,z,t)\big|_{\Gamma_1} = H(x,y,z,t) & (x,y,z) \in \Gamma_1 \\[4pt]
K_{xx}\frac{\partial H}{\partial x}\cos(n,x) + K_{yy}\frac{\partial H}{\partial y}\cos(n,y) + K_{zz}\frac{\partial H}{\partial z}\cos(n,z)\Big|_{\Gamma_2} = q(x,y,z,t) & (x,y,z) \in \Gamma_2 \\[4pt]
H(x,y,z,t) = & (x,y,z) \in \Gamma_3
\end{cases}
\tag{1}
$$

where K_{xx}, K_{yy} and K_{zz} are the hydraulic conductivities of the principal directions for the anisotropic aquifers. $H(x, y, z)$ is the hydraulic head value at the instant t. W is the source and sinks term. t is the time. S_s is the specific storage. Ω is the computational domain. $H_0(x, y, z, t_0)$ is the initial water level. The recharge capacity per unit area for the second boundary condition is given by $q(x, y, z, t)$ and $\cos(n, x)$, $\cos(n, y)$, and $\cos(n, z)$ are the directional cosines for the normal to the body surface. Γ_1, Γ_2 and Γ_3 are the first, second and free surface boundary conditions, respectively.

The finite element discretization of Equation (1) can be given as an algebraic equation for the seepage flow domain:

$$[G]\{H\} + [P]\left\{\frac{dH}{dt}\right\} = \{F\} \tag{2}$$

$$\frac{dH}{dt} = \frac{H(t+\Delta t) - H(t)}{\Delta t} \tag{3}$$

$$[G]\{H_{t+\Delta t}\} + [P]\left\{\frac{H(t+\Delta t) - H(t)}{\Delta t}\right\} = \{F\} \tag{4}$$

where $[G]$ is the seepage matrix, $\{H\}$ is the hydraulic head matrix, $[P]$ is the storage matrix, and $\{F\}$ is the known right-hand member.

3.2. Model Calibration Method

The difference between the calculated and observed values in the model is estimated using root mean squared error (RMSE) as the mean average of the squared differences, and the minimum sum of squares of the groundwater level (H) residual is used as the objective function: $\min E = \| H_c - H_0 \|^2$. Thus,

$$E\left(K_j^i\right) = \sum_{k=1}^{M} \sqrt{\left(H_k^c - H_k^o\right)^2} \tag{5}$$

where K_j^i is the pending parameters for different material partitions. H_k^c and H_k^o are the calculated and observed groundwater level values, respectively.

3.3. Conceptual Model

(1) Model Scope

The aquifer system of this simulation mainly includes the phreatic aquifer in the Quaternary loose rock pervious aquifer, the first confined aquifer, second confined aquifer, and third confined aquifer, and three aquitards between each aquifer. Considering the geological conditions of the study area and the data from the pumping tests, the aquifer system is generalized as heterogeneous anisotropy, and the horizontal permeability (1.0–5.0 m/day) is greater than the vertical permeability (0.1–0.5 m/day). According to the borehole-log lithology records and the in situ pumping tests, the influence radius is between 320.15 and 565.25 m. Considering the hydrogeological conditions and the errors in the pumping test, the simulation scope is 1 km around the emergency groundwater source. The model calculation area is shown in Figure 7.

(2) Initial and Boundary Conditions

The stream was usually set as the boundary condition, that is, the model scope should not exceed the Tonglu River. The pumping was conducted in the third confined aquifer, but there was no hydraulic connection with the stream, so the stream should not be considered as the evaluation scope. In addition, the recharge between the stream and the phreatic aquifer was through the streambed. The boundary around the study area was the first boundary type. Considering that the influence scope of pumping was small, the water head around the model was treated as a constant. The top boundary of the model was a recharge boundary for precipitation, and also a discharge boundary for evaporation so it was treated as a free surface boundary. The bottom boundary was treated as the impervious boundary,

which was the lower interface in the third confined aquifer. The initial water level of the simulation prediction was determined by the water level of the monitoring well in each aquifer, and the initial water level of the entire simulation area was obtained by interpolation. Let the center of the water source be the origin of coordinates in the calculation area, the positive direction of the *y*-axis along the due north, the positive direction of the *x*-axis along the due east, and the positive direction of the *z*-axis along the vertical upward. Considering the geological setting and the relatively large thickness of the aquifer, the model was divided into seven layers in the vertical direction, namely, three aquitards and four aquifers. The model domain was discretized using triangular elements with 97,352 nodes in each slice and 169,358 elements in each layer.
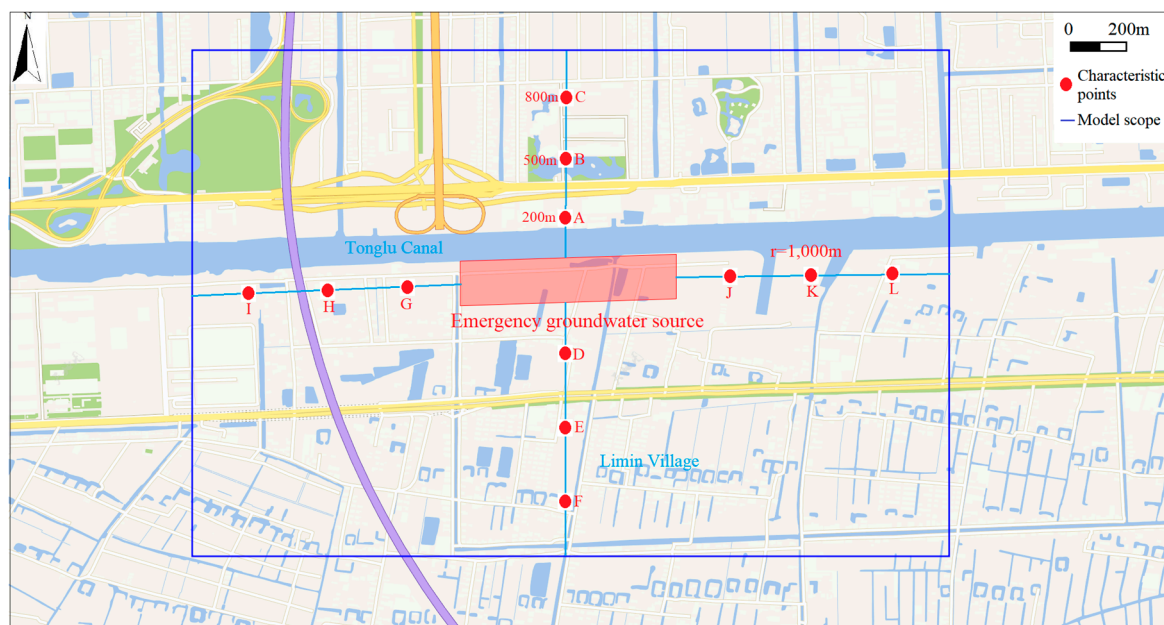

Figure 7. Model calculation area.

3.4. Field Tests and Parameters Determination

(1)　Permeability test in streambed sediments

The permeability test was mainly used to determine the hydraulic connection between the surface water (Tonglu Canal water) and the phreatic aquifer and to quantitatively calculate the hydraulic conductivity of the streambed sediments in the study area. The Figure 8 showed a vertical standpipe in the stream channel, where the lower part of the pipe had been pressed into the streambed and was filled with the unconsolidated sediment. Water was poured into the pipe to fill the rest of the pipe. Then, head losses in the pipe were measured at different times. The water level at the bottom of the sediment column was approximately equal to the water level in the stream. Because of the difference in water levels at the two ends of the sediment column in the pipe, water flowed through the sediment column, and the water table in the pipe fell. The standpipe test used polyvinyl chloride (PVC) pipe with a length of 2 m. Due to the test lasted for a long time, to ensure that the water level in the pipe would not change due to other conditions and cause inaccurate data, the top of the pipe was sealed with a thin film to prevent evaporation or precipitation.

According to the research result of Chen [52], K_v can be determined as

$$K_v = \frac{L_v}{t_1 - t_2} \ln \frac{h_1}{h_2} \qquad (6)$$

where K_v is the vertical hydraulic conductivity of the streambed sediments. L_v is the thickness of the measured streambed sediments in the pipe. h_1 and h_2 are the water head in the pipe at time t_1 and t_2, respectively. It was assumed that the river stage was constant during the test.
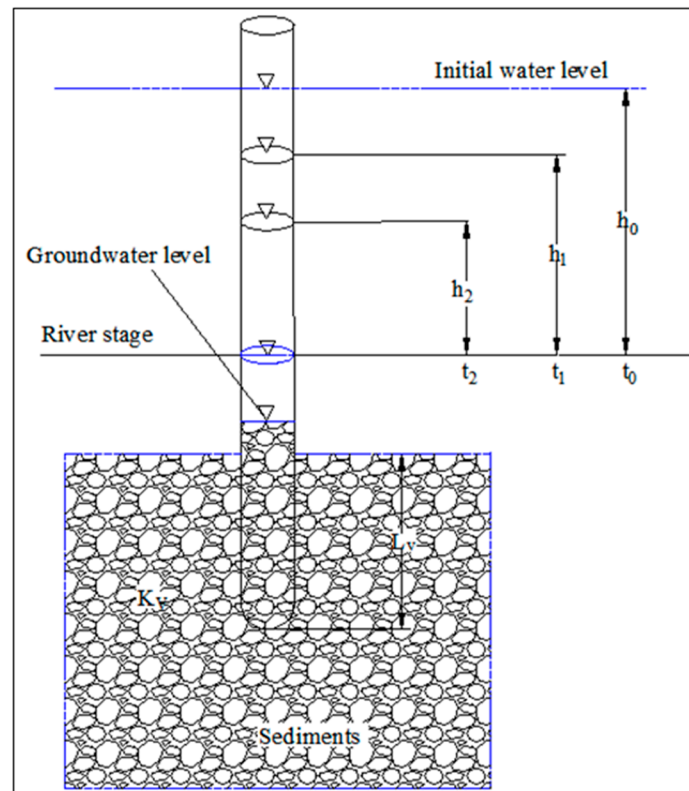

Figure 8. Schematic diagram of the permeability test in streambed sediments.

On the north side of the study area, a vertical standpipe was inserted to conduct two permeability tests in Tonglu Canal, one for K_{v1} and the other for K_{v2}. The position coordinates of vertical standpipe for the first test were 32°2′39.32″ N, 120°58′43.31″ E. The upper part of the pipe was 21 cm away from the river stage and L_{v1} was 41 cm. The observation time was 45 h from 2 November to 4 November. The calculated value of hydraulic conductivity was between 3.83×10^{-7} and 1.11×10^{-6} m/s, and the average value was 6.95×10^{-7} m/s, namely 0.06 m/day. The position coordinates of vertical standpipe for the second test were 32°2′39.22″ N, 120°58′40.22″ E. The upper part of the pipe was 91 cm away from the river stage and L_{v2} was 50 cm. The observation time was 45 h. The calculated value of hydraulic conductivity was between 6.23×10^{-8} and 5.01×10^{-7} m/s, and the average value was 4.68×10^{-7} m/s, namely, 0.04 m/day. According to the results of two tests, the average hydraulic conductivity was 0.05 m/day.

(2)　Pumping tests

Pumping tests were conducted to determine the hydrogeological parameters of the aquifer and the hydraulic relationship between the aquifers in test boreholes, numbered as J_1 and J_2. The borehole depth of J_1 was 294 m, the range of depth of pumping level was from 270 m to 290 m, and the borehole depth of J_2 was 300 m, and the pumping level ranges from 204 to 212 m and 276 to 288 m. The observation and recording time of pumping test data was 1 min, 3 min, 5 min, 10 min, 20 min, 30 min, 1 h, and then recorded every other hour. After three tests, if the data obtained was the same or the water level difference did not exceed 2 cm within 4 h, the pumping test was considered stable and could be stopped. After that, the water level recovery observation was needed. The time interval was 1 min, 3 min, 5 min, 10 min, 20 min, 30 min, until the complete recovery. The pumping and

recovery test data are shown in Table 1. The calculated hydraulic conductivities were 1.46 and 2.65 m/d, respectively. Since the third confined aquifer was mainly composed of medium-fine sand and silt fine sand, the hydraulic conductivity of the third confined aquifer was between 1.0 and 5.0 m/d.

(3)　Determination of Influence Radius

Table 1. Statistics parameters of pumping and recovery water tests.

Well Number	Static Level (m)	Dynamic Level (m)	Drawdown (m)	Pumping Rate (m³/day)	Water Temperature (°C)	Stable Time (h)	Recovery of Water Levels (m)	Recovery Time of Water Level (h)
J_1	−22.85	−28.92	5.07	1920	22	25	−22.95	3.5
J_2	−22.65	−26.95	4.0	1920	22	25	−22.85	3.5

The third confined aquifer was divided into upper and lower sections. The upper section was composed of fine sand and medium-fine sand, with a thickness between 13 and 21 m; the lower section was gravel-bearing medium-coarse sand with a thickness between 26 and 30 m. The permeability and water yield properties of the two sections were relatively high. Using J_1 as a pumping well and J_2 as an observation well to conduct in situ pumping tests, and then using the results of the pumping tests to calculate the influence radius when a single well is pumped, as follows:

$$\lg R = \frac{s_w \lg r_1 - s_1 \lg r_w}{s_w - s_1}$$

(7)

where R is the radius of influence. s_w is the drawdown of the pumping well. r_1 is the distance from the observation well to the pumping. r_w is the radius of the pumping well. s_1 is the drawdown of the observation well. The radius of the well in this pumping test is 0.3 m. When the pumping rate is 80 m³/h, the steady drawdown of the pumping well is 5.07 m, the drawdown of the observation well is 0.47 m, and the distance between wells is 127.3 m, so the calculated influence radius is 148.65 m.

Considering that 13 wells working at the same time during the operation of the groundwater source, which the influence radius of them was larger than that of a single well for pumping tests, so the "large-well method" could be used to calculate the influence radius for multi-well tests. The "large-well method" was to simplify the area occupied by the gallery pattern system into a large well in the prediction of discharge rate, and then apply the method of groundwater dynamics to calculate the influence radius and predict the discharge rate of the gallery pattern system. The r_0 can be expressed as

$$r_0 = \eta \frac{a+b}{4}$$

(8)

where r_0 is the reference radius, a is the length of the multi-well area, b is the width of the multi-well area, and the values of η, a, and b are shown in. The length and width of the multi-well area are 801.77 and 190.17 m, respectively. According to the Table 2, η is 1.12, that is, r_0 is 277.74 m. The influence radius of large well is calculated using the formula for steady flow to a confined aquifer, and the influence radius of R_0 is between 320.15 and 565.25 m.

Table 2. Relationship of η and a/b.

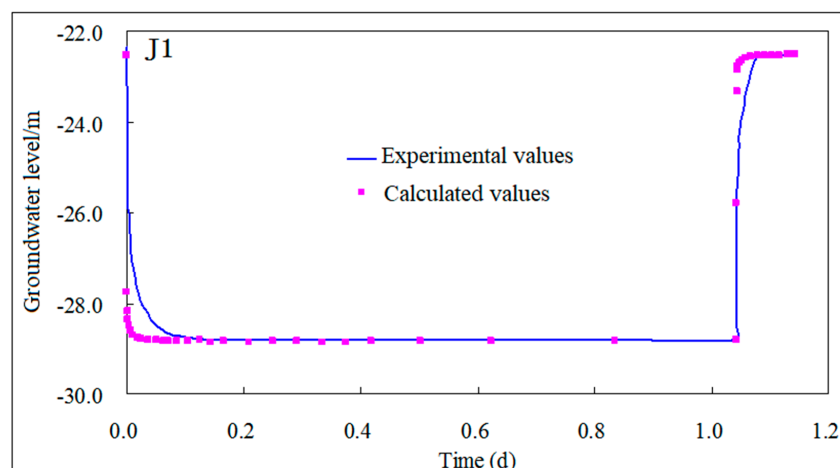| a/b	0	0.2	0.4	0.6	0.8	1.0
η	1.00	1.12	1.14	1.16	1.18	1.18

3.5. Model Calibration

According to the characteristics of heterogeneity and anisotropy of the study area, combined with the stratum lithology distribution, the water yield property of the aquifer, and other conditions, the study area was divided into four aquifers on the profile (phreatic aquifers, first confined aquifer,

second confined aquifer, and third confined aquifer) and three impermeable aquifers (clay loam layer). The hydraulic conductivity obtained from the pumping water tests, recovery water tests and the empirical hydraulic conductivity of each soil layer was taken as the initial values of the model parameters. The initial values of hydraulic conductivity for different aquifers were shown in Table 3. The initial value of the model was verified using Equation (5) in Section 3.2. By comparing the experimental drawdown of the pumping wells with the calculated drawdown, and the flow model parameters were obtained by numerical reverse analysis. The water level fitting curve was shown in Figure 9. It can be seen in Figure 9 that the measured value of the drawdown in 4 to 12 h of pumping test fits well with the calculated value. The initial stage of the pumping test was poor, but the overall variation tendency remained consistent. The inversion parameters can reflect the permeability of the aquifer. The inversion values of hydraulic conductivity for different aquifers were shown in Table 4.
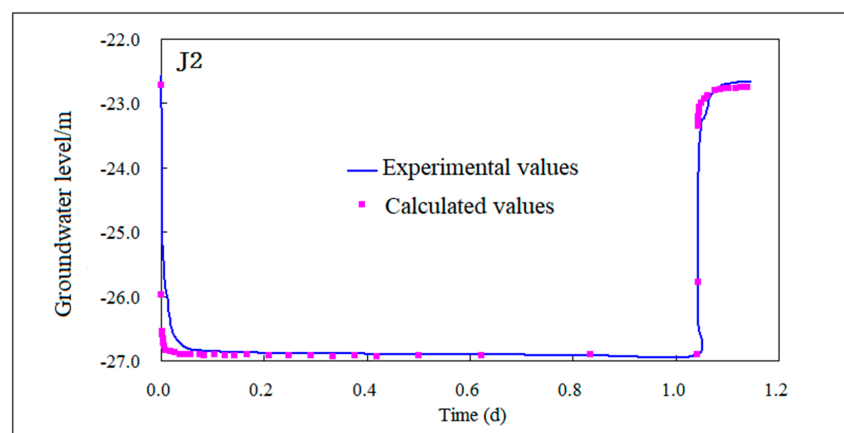
Table 3. Initial values of hydraulic conductivity for different aquifers.

Aquifer Types	Hydraulic Conductivity K (m/day)
Phreatic aquifer	0.5–5.0
1st CA [1]	1.0–5.0
2nd CA	0.5–1.0
3rd CA	1.0–5.0
Aquitard	0.02–0.5

[1] CA means confined aquifer.

(a)

(b)

Figure 9. Fitting curves of experimental and calculated groundwater levels from pumping test ((**a**) Pumping test well J1, (**b**) Pumping test well J2).

Table 4. Inversion values of hydraulic conductivity for different aquifers.

Aquifer Types	Hydraulic Conductivity(m/day)		
	K_{xx}	K_{yy}	K_{zz}
Phreatic aquifer	1.5	1.5	0.15
Aquitard	0.03	0.03	0.003
1st CA [1]	3.5	3.5	0.35
Aquitard	0.02	0.02	0.002
2nd CA	5.0	5.0	0.5
Aquitard	0.03	0.03	0.003
3rd CA	4.8	4.8	0.48

[1] CA means confined aquifer.

4. Results Analysis and Discussion

4.1. Prediction of Groundwater Level during Pumping and Recovery Tests

During the operation of the emergency groundwater source, in addition to the existing 2 test wells, 11 new wells were added, numbered as J_3 to J_{13}. The pumping rate of each well was about 1920 m^3/day, and the total pumping rate was about 25,000 m^3/day. All emergency wells exploited groundwater in the third confined aquifer.

(1)   Prediction of groundwater level during pumping

After surface water was contaminated, the time from emergency treatment to water supply resumption generally did not exceed seven days. Therefore, the maximum time for emergency pumping was set to seven days, 13 wells were working at the same time, and the total pumping rate was about 25,000 m^3/day. The calibrated groundwater flow numerical model was used to predict groundwater level change after pumping as shown in Figure 10.

It can be seen from Figure 10 that the drawdown was the most at the multi-well, and a cone of depression was formed there. With the increase of pumping time, the cone of depression gradually spread to the surrounding area. After seven days of emergency pumping, the cone of depression expanded to the boundary. It can be seen from Figure 7 that after 1, 3, 5, and 7 days of pumping, the lowest water level in the center of the depression cone was about −42.11, −49.17, −52.64, and −55.82 m, and the maximum drawdown 19.11, 26.17, 29.64, and 32.82 m, respectively.

The water level changes around the emergency groundwater source can be analyzed by taking characteristic points (Figure 7). Three characteristic points (A–L) were taken from the north, south, west, and east of the water source. The distances from the boundary of the water source are 200, 500, and 800 m, respectively. The calculated water level is shown in Table 5. It can be seen the closer to the water source, the more the drawdown and vice versa. When pumping for five days, the dynamic water level change at 200 m from the water source boundary exceeded −35 m, and the dynamic water level change at 500 m and 800 m from the water source boundary was much lower than the warning stage, which is −35 m.

To understand the changing trend of the groundwater level in the center of the depression cone in the profile, three different profiles were taken for research. The groundwater level change with time was shown in Figure 11. It could be seen that the groundwater level in the center of the depression cone ranged from −51 m to −56 m after seven days of pumping. Compared with the initial water level, the drawdown was about 29–32 m. Among them, the J5-J9 pumping wells located in the center of multi-well had the largest drawdown, with a value of −55 m. The water level of the remaining wells was about −52 m. The water level between the two pumping wells was generally −42 m to −45 m. Based on the principles of groundwater dynamics and using the analytical formula for pumping test from multi-well, the drawdown of 13 wells during the pumping could be calculated, which was between 28.5 m and 31.26 m. The results were consistent with the numerical results, which indicated that the prediction results were reasonable.
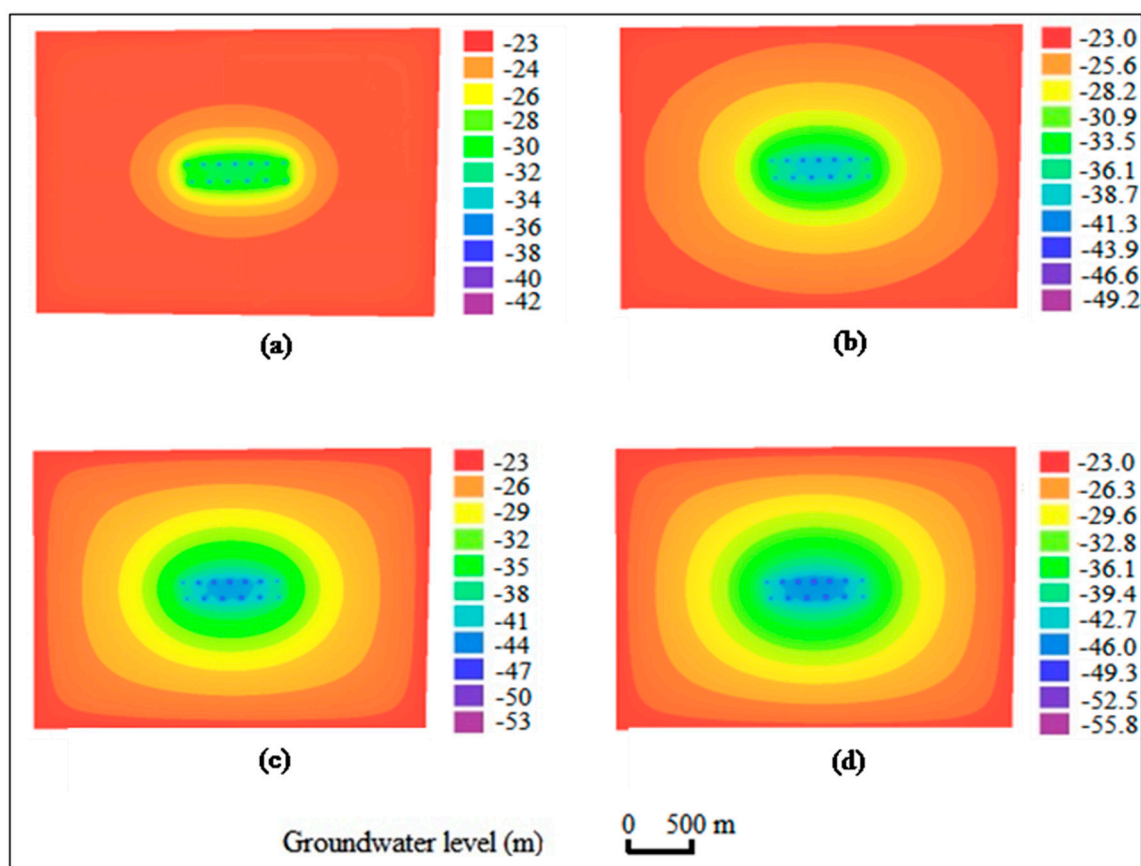
Figure 10. Contour maps of groundwater level in the third confined aquifer during pumping. (**a**) emergency groundwater supply day 1, (**b**) emergency groundwater supply day 3, (**c**) emergency groundwater supply day 5, and (**d**) emergency groundwater supply day 7.

Table 5. Statistics of groundwater level changes around the water source during pumping.

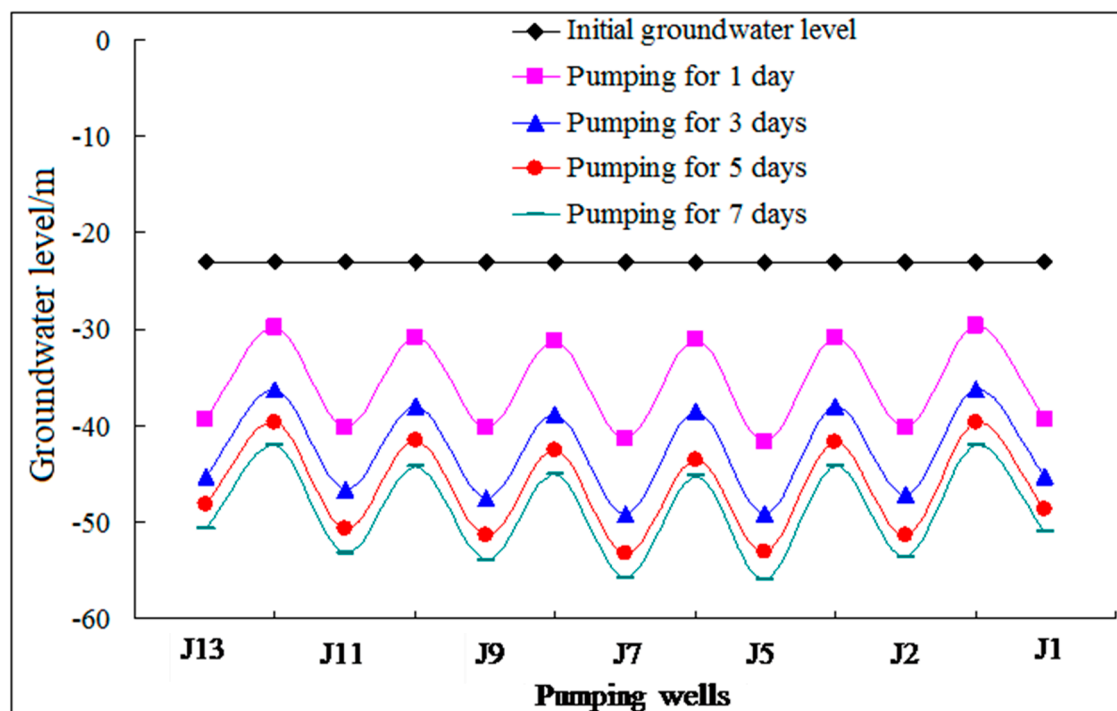| Point Position	The Distances from the Boundary of the Water Source (m)	Groundwater Level after Pumping for a Certain Time (m)			
		1 day	3 days	5 days	7 days
A	200	−26.41	−32.21	−36.90	−38.56
B	500	−24.16	−26.65	−29.87	−29.61
C	800	−23.65	−24.11	−24.53	−25.48
D	200	−26.21	−32.75	−36.78	−38.24
E	500	−24.21	−26.76	−29.70	−29.56
F	800	−23.84	−24.36	−24.68	−25.26
G	200	−25.35	−29.89	−32.16	−34.32
H	500	−24.14	−26.01	−27.76	−28.68
I	800	−23.92	−24.18	−24.49	−24.71
J	200	−25.61	−30.13	−32.96	−34.16
K	500	−24.12	−26.14	−27.69	−28.54
L	800	−23.67	−24.14	−24.26	−24.58

(2)   Prediction of groundwater level during recovery tests

When the emergency groundwater source operated for seven days, the pumping was stopped, and the water level of the pumping well and its surroundings rose rapidly (Figures 12 and 13). On the 1st, 5th, 10th, 15th, 20th, and 30th day during water level recovery, the water level in the center of the depression cone were −42.07, −33.13, −30.16, −26.58, −24.51, and −23.28 m, respectively. Compared with the seventh day of pumping, the water levels increased by 13.75, 22.69, 25.66, 29.24, 31.31, and 32.54 m, respectively. It can be seen that the rising process of water level was fast and then slow.

When the water level recovery was for five days, the lowest water level was −33.13 m. After 30 days of water level recovery, the difference from the initial water level was about 0.28 m. It indicated that the groundwater recovered to the state before pumping (Table 6).
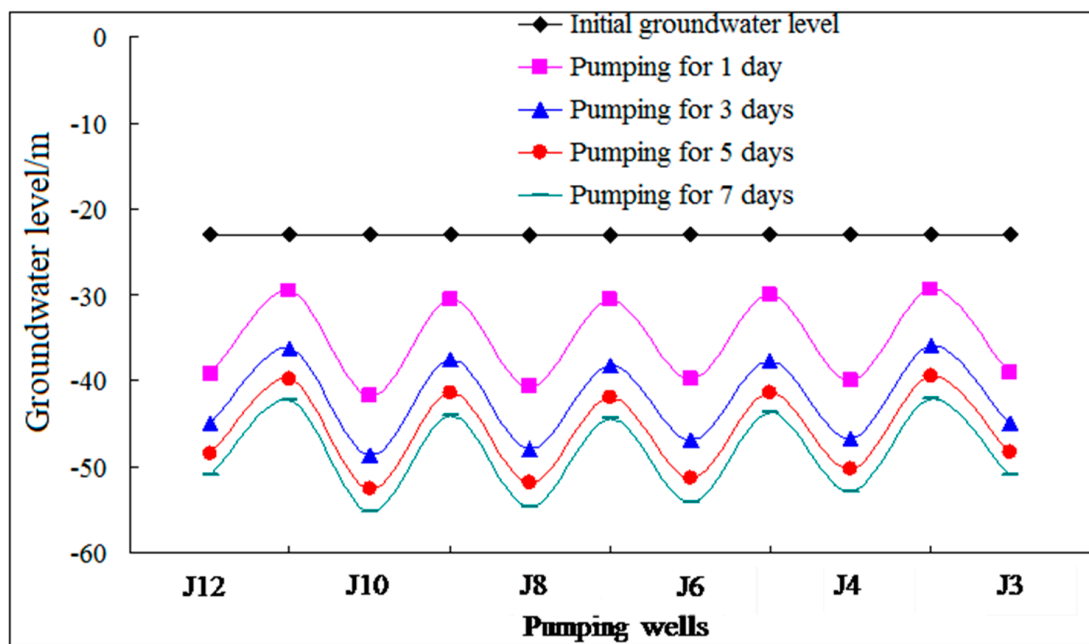
Table 6. Statistics of groundwater level changes around the water source during water level recovery.

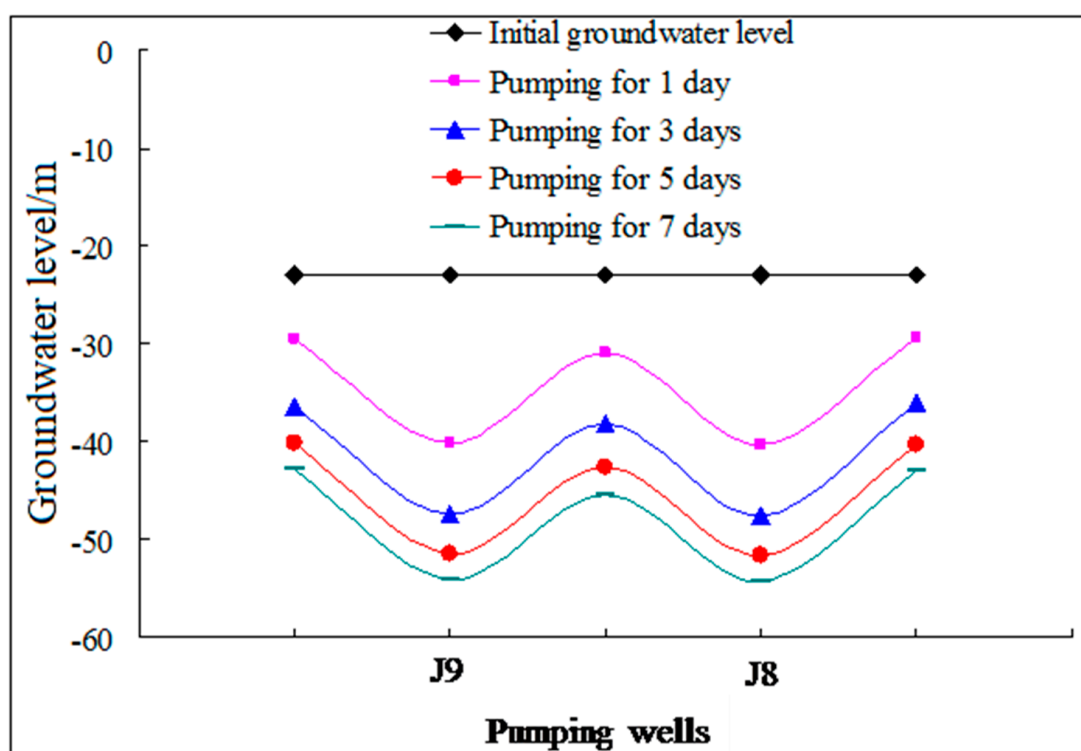| Point Position	The Distances from the Boundary of the Water Source (m)	Groundwater Level Recovery for a Certain Time (m)					
		1 day	5 days	10 days	15 days	20 days	30 days
A	200	−37.68	−32.67	−28.90	−26.48	−24.37	−23.26
B	500	−28.95	−26.93	−25.53	−24.98	−23.89	−23.16
C	800	−24.72	−24.29	−23.96	−23.74	−23.22	−23.04
D	200	−37.79	−32.56	−28.76	−26.36	−24.16	−23.24
E	500	−29.04	−26.83	−25.52	−24.85	−23.73	−23.12
F	800	−24.93	−24.26	−23.91	−23.57	−23.24	−23.05
G	200	−33.44	−30.32	−28.20	−26.14	−24.34	−23.26
H	500	−27.35	−26.55	−25.97	−24.59	−23.90	−23.18
I	800	−24.23	−24.02	−23.84	−23.71	−23.19	−23.07
J	200	−33.48	−30.16	−28.36	−26.15	−24.26	−23.24
K	500	−27.17	−26.53	−25.86	24.42	−23.74	−23.17
L	800	−24.29	−24.63	−24.36	−23.69	−23.16	−23.09

(a)

Figure 11. *Cont.*

(**b**)

(**c**)

Figure 11. Curves of the cone of depression during pumping ((**a**) Section J13-J1, (**b**) Section J12-J3, (**c**) Section J9-J8).
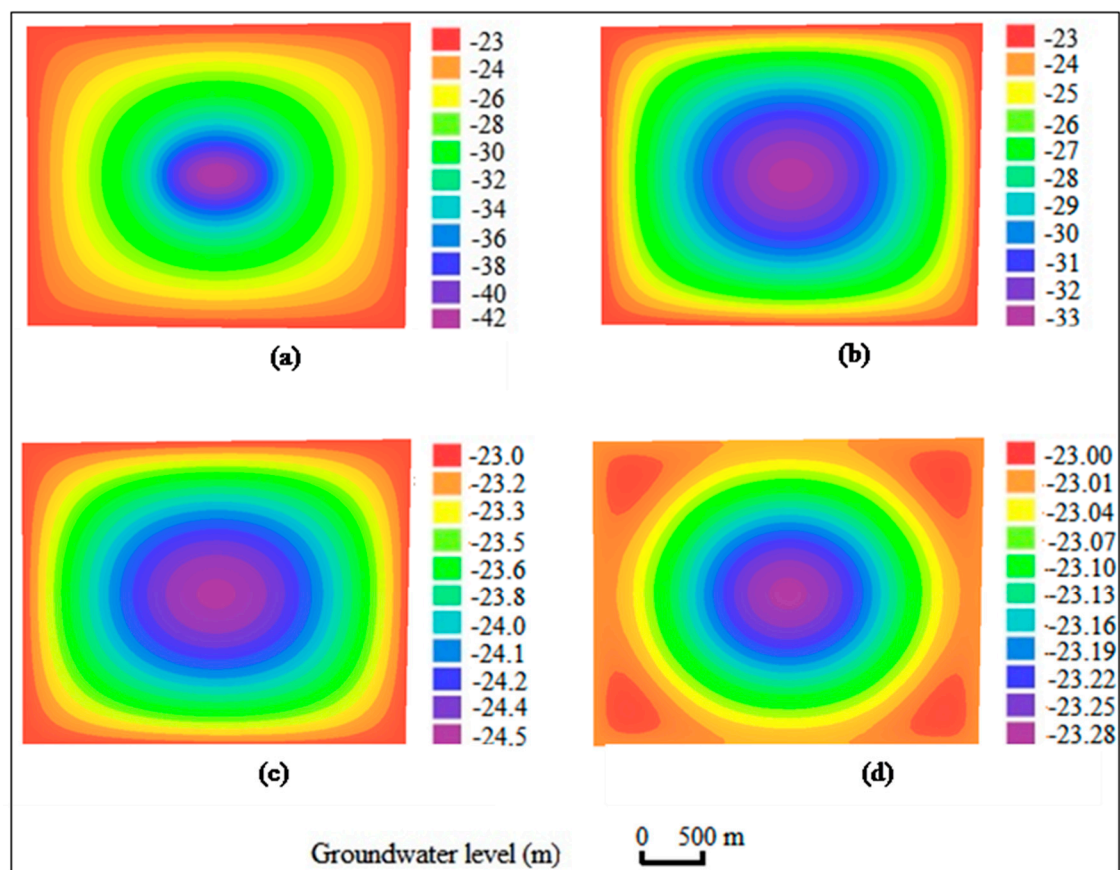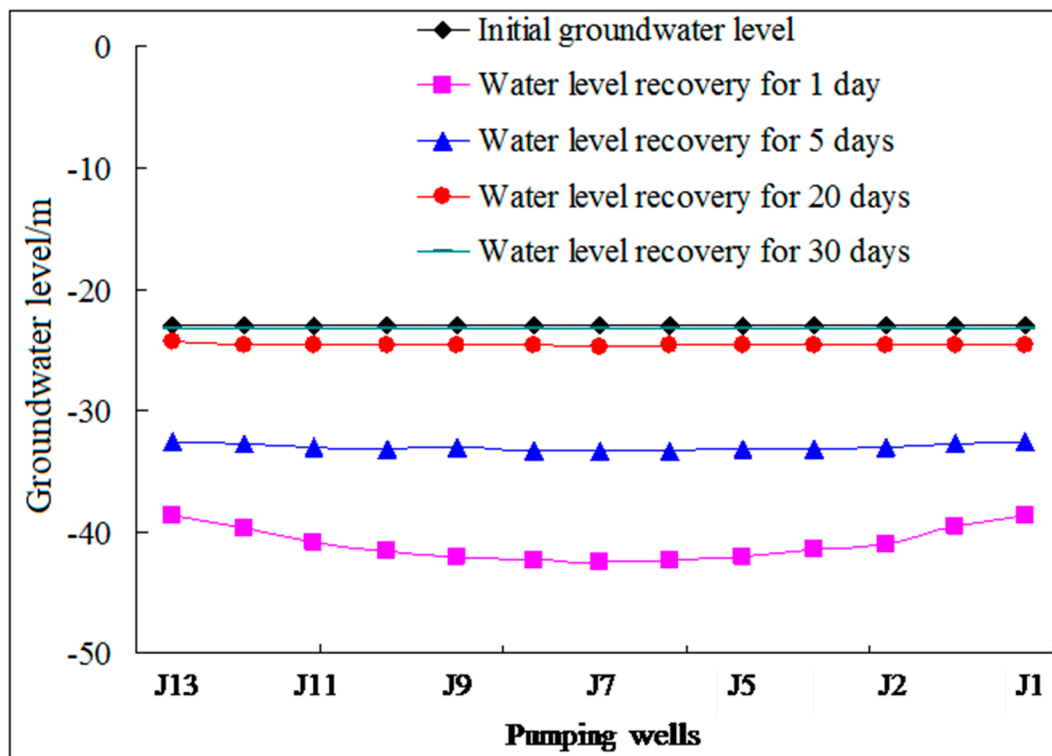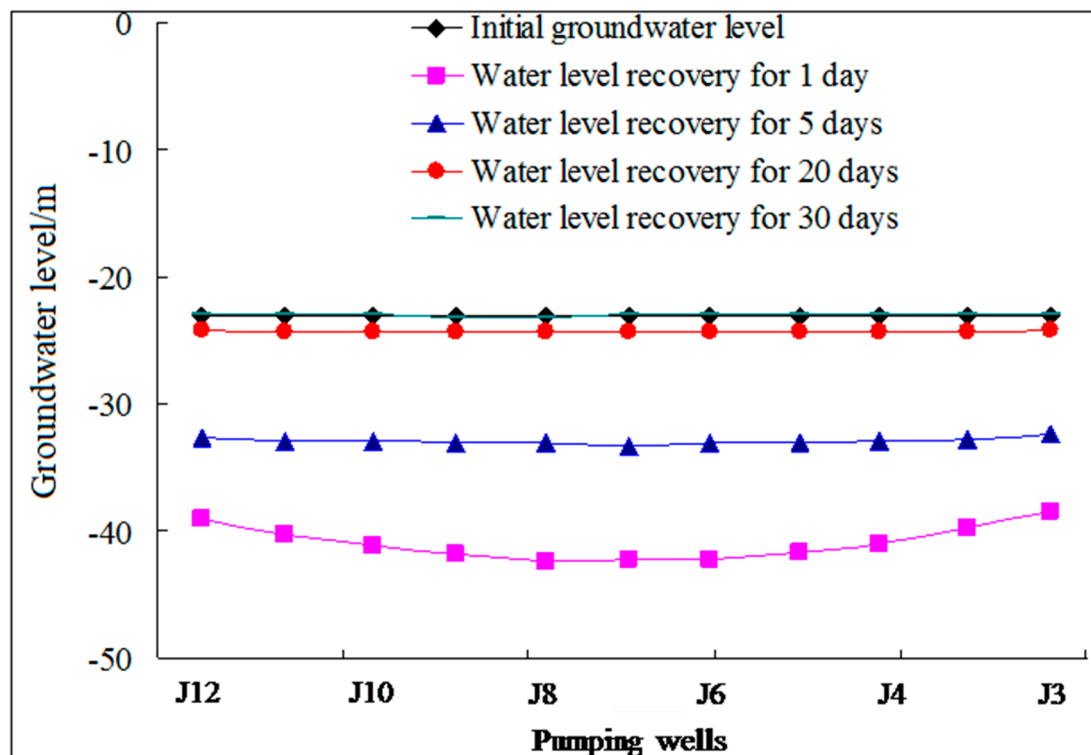
Figure 12. Contour maps of groundwater level in the third confined aquifer during water level recovery ((**a**) water level recovery day 1, (**b**) water level recovery day 5, (**c**) water level recovery day 20, and (**d**) water level recovery day 30).

(**a**)

(**b**)

Figure 13. Cone depressions during pumping ((**a**) Section J13-J1, (**b**) Section J12-J3).

4.2. Impact of Emergency Water Sources on the Surrounding Environment during Operation

(1)   Analysis of impact on Tonglu Canal

Tonglu Canal flows near the emergency groundwater source, and the distance from the pumping well is about 20 m. Tonglu Canal is at the proposed location of the Limin village project. The normal water level, the warning water level, the highest water level on records, and the floodwater level in a one-hundred-year return period of the canal were 2.21, 2.61, 3.35, and 3.65 m, respectively. The streambed elevation was −2.10 m and the thickness of streambed sediments ranges from 40 to 100 cm. The permeability was low and the hydraulic conductivity was 0.05 m/day. There was a certain hydraulic connection between Tonglu Canal and phreatic water, and the recharge between them had been considered in the numerical simulation. The emergency groundwater source was located at the third confined aquifer, which is deeply buried. There were three aquitards between phreatic water and third confined water. Therefore, pumping in the third confined aquifer for a short time would hardly affect the phreatic aquifer. That was to say, pumping in the third confined aquifer had no impact on Tonglu Canal.

(2)   Analysis of impact on the surrounding residential wells

At present, the drinking water of the surrounding residents in the project area mainly is from surface water, but some villagers still keep residential wells, which are mainly used for washing clothes, watering vegetables, and livestock water. These residential wells are shallow and are generally distributed in the phreatic aquifer and the first confined aquifer. When pumping in the third confined aquifer, the hydraulic connection between the phreatic water, the first confined aquifer and third confined aquifer is weak, so it will not cause the drawdown in the residential wells. Moreover, there are thicker, low permeability clay or clay loam impervious layers between the aquifer formation in the deep groundwater. The hydraulic connection and the leakage effect between the aquifers are weak. Therefore, groundwater exploitation in the third confined aquifer will not have a significant impact on the phreatic aquifer and the first confined aquifer. It should be pointed out that this prediction came from the model results and analysis of hydrogeological conditions. In the future, more observation wells are needed to confirm our findings.
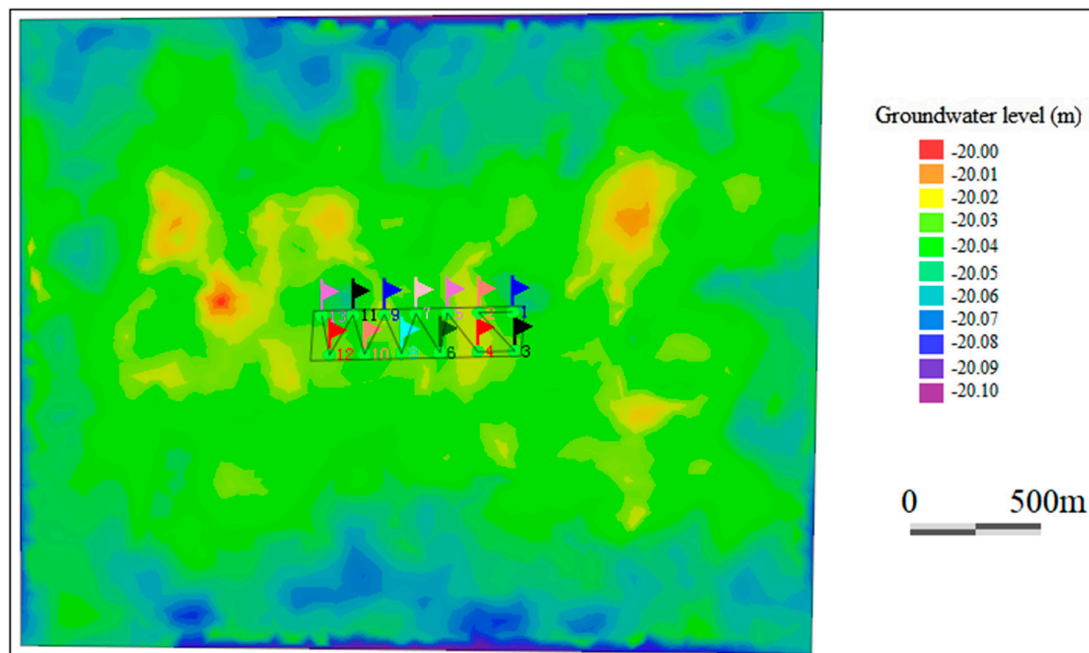
(3)   Analysis of impact on the second confined aquifer

The depth of the static level and the upper interface of the second confined aquifer range from 3.0 to 5.0 and 130 to 150 m, respectively. The lithology of the aquifer is fine sand with a thickness of 25–30 m. According to subsurface data [53], there is a stable distribution of tight silty clay impervious layer with a thickness of 40–50 m between the second confined aquifer and the third confined aquifer, so the hydraulic connection between the two aquifers is relatively weak. The results of numerical simulation also show that the water level in the second confined aquifer has not changed after seven days of pumping, and it is not affected by the pumping results of the third confined aquifer (Figure 14). It should be pointed out that this conclusion is based on the discussion of numerical simulation. The second confined aquifer did not have the observation well, so more groundwater level changes in the second confined aquifer needed to be verified through observation wells. In addition, due to the barrier effect of the silty clay, the saltwater in the second confined aquifer is also difficult to enter the third confined aquifer, so the water quality of the third confined aquifer will not be affected.
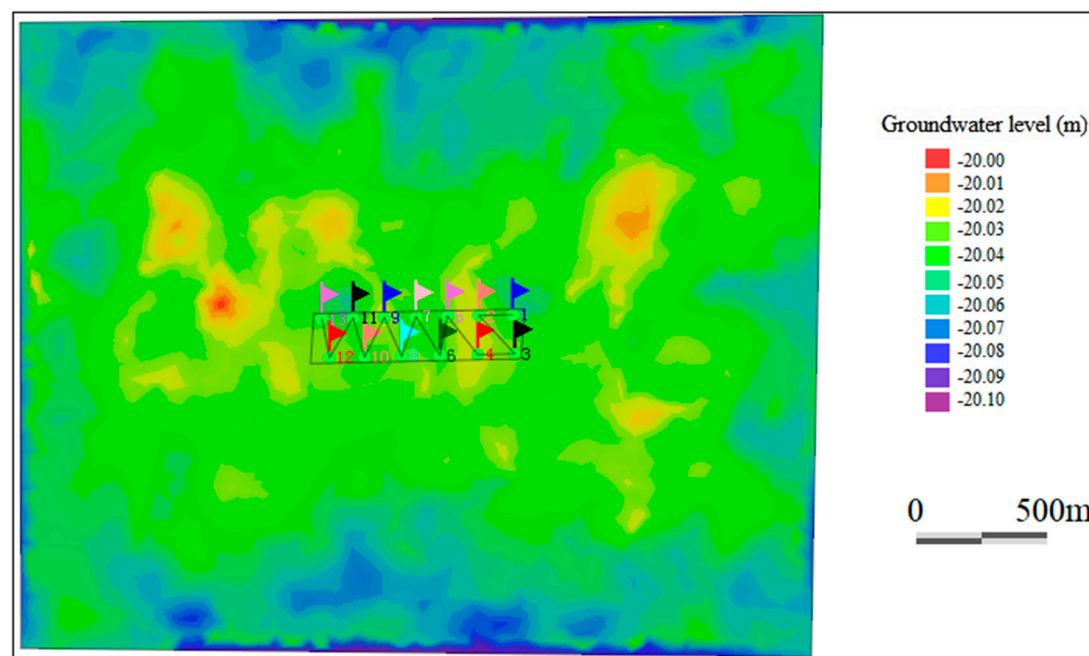
(4)   Analysis of impact on land subsidence

Regional data show that the stratum in this area is relatively soft and easily compressed to cause land subsidence. The total settlement of soil layers is equal to the sum of the settlement of each soil layer. The subsidence at the wall of the pumping well is caused by the drop in the groundwater level. There is no drawdown above the groundwater level, so the land subsidence is neglect. However, the sand or clay layer below the initial water level can cause land subsidence. Therefore, the land subsidence caused by the pumping well occurs in the part of the initial water level to the lower interface of the aquifer. According to the rock formation type and data, the empirical value is selected for calculation. When the maximum drawdown is 32 m, the total settlement is about 27.33 mm (where the

total thickness of the water-bearing sand layer and clay layer are 90 and 184 m, respectively; the initial water level is about above 26 m). The third confined aquifer formation is composed of the Lower Pleistocene series (Q_1) strata and has a relatively compact structure and low compressibility. Therefore, during the operation of the emergency groundwater source, a large area of land subsidence will not occur due to larger drawdown.

(**a**) Initial groundwater level

(**b**) Pumping for 7 days

Figure 14. Groundwater level of the second confined aquifer.

In addition, due to local governments restricting groundwater exploitation in recent years, the groundwater level has risen significantly. This measure has effectively controlled the problem of land subsidence. The results showed that during the operation of the emergency groundwater source

for seven days, the groundwater level in the center of the depression cone dropped to about −55.82 m (Figure 15), which exceeded the warning water level (namely −35 m) by 20.82 m. If this is maintained for a long time, the water level will be difficult to recover and may cause land subsidence. However, the emergency groundwater source of this project has been operating for less than seven days, and the water level rises quickly during water recovery, so the water level change in a short time will not cause land subsidence.

Figure 15. Change curves of groundwater level in the center of depression cone during the operation of emergency groundwater source.

5. Conclusions

The numerical methods are used to predict the change of groundwater level during the operation of emergency groundwater sources and the analysis of its impact on the surrounding environment. The main conclusions drawn from this study are as follows:

(1) According to the vertical standpipe test, the vertical hydraulic conductivity of the streambed sediments was 0.05 m/day, and the hydraulic conductivity of the aquifer was 1.0–5.0 m/day obtained through the pumping test. These parameters were taken as the initial values of the model parameters. Based on the water level of the pumping test and the calculated water level, the established numerical model was calibrated. The calibrated model was used to predict the changes in the groundwater level during pumping and water level recovery.

(2) Numerical results show that the groundwater level at the pumping well had the largest drawdown and a cone of depression was formed there. After seven days of pumping, the water level in the center of the depression cone ranged from −51 to −55 m and compared with the initial water level, the water level dropped by 29 to 32 m. Among them, the J5-J9 located in the center of the multi-well had the largest drawdown, and the water level at the other pumping wells had a small drawdown, which was consistent with the results of the analytical solution; In addition, during water level recovery, the water level of pumping wells and its surroundings rose rapidly, which was a difference of about 0.28 m from the initial water level after 30 days, indicating that the groundwater level had recovered to the state before pumping.

(3) The vertical hydraulic conductivity of the streambed sediments calculated by the vertical standpipe test was small, indicating that the Tonglu Canal had a certain hydraulic connection with the phreatic water. However, the emergency groundwater source was located at the third confined aquifer which was buried depth, and there were three aquitards between phreatic water and

third confined water; therefore, the pumping in the third confined aquifer had no impact on the Tonglu Canal. The residential wells around the emergency water source are shallow and generally distributed in the phreatic aquifer. When pumping in the third confined aquifer, the hydraulic connection between phreatic water and the third confined aquifer was weak, so it would not cause any apparent drawdown in the residential wells. The numerical results also showed that the water level in the second confined aquifer had not changed after 7 days of pumping, and was not affected by the pumping results of the third confined aquifer. During the operation of the emergency groundwater source for seven days, the groundwater level in the center of the depression cone dropped to about −55.82 m, which exceeded the warning water level (namely, −35 m) by 20.82 m. If this is maintained for a long time, the water level will be difficult to recover and may cause land subsidence. However, this project has been operating for less than seven days, and the water level recovers quickly, so the change of water level in a short time will not lead to large land subsidence and has little impact on the surrounding environment.

Overall, the change of groundwater level of the emergency water source in Nantong during the emergency pumping period and recovery period was predicted accurately by numerical method. The normal operation of the emergency water source had low impact on the surrounding environment. At the same time, the impact on the surrounding environment need to be confirmed by setting up more observation wells in the future. In addition, due to the different geological conditions, climatic conditions and economic development conditions of each emergency water source, our research results were limited and preliminary. Further research is needed to assess the impact of emergency pumping on the migration of pollutants.

References

1. Carrard, N.; Foster, T.; Willetts, J. Groundwater as a Source of drinking water in southeast Asia and the Pacific: A multi-country review of current reliance and resource concerns. *Water* **2019**, *11*, 1605. [CrossRef]
2. Zhou, Y.; Wu, F.P.; Chen, Y.P. Emergency reserved water demand estimation for public events of accidental water source pollution. *J. Nat. Resour.* **2013**, *28*, 1426–1437.
3. Scawthorn, C.; Ballantyne, D.B.; Blackburn, F. Emergency water supply needs lessons from recent disasters. In *Water Supply*; Tokyo, Japan, 15–18 November 1998; IWA Publishing: London, UK, 2000; Volume 18, pp. 69–77.
4. Vizintin, G.; Ravbar, N.; Janez, J.; Koren, E.; Janez, N.; Zini, L.; Treu, F.; Petric, M. Integration of models of various types of aquifers for water quality management in the transboundary area of the Soca/Isonzo river basin (Slovenia/Italy). *Sci. Total Environ.* **2018**, *619*, 1214–1225. [CrossRef] [PubMed]
5. Zhao, S.; Huang, B.; Guo, B. Water Environment Prediction and Evaluation on Reservoir Dredging and Source Conservation Project-Case Study of Duihekou Reservoir. In *Communications in Computer and Information Science, Proceedings of the 3rd Annual International Conference on Geo-Informatics in Resource Management and Sustainable Ecosystem (GRMSE), Wuhan, China, 16–18 October 2015*; Springer: Cham, Switzerland, 2016; Volume 569, pp. 520–524.
6. Sheriff, J.D.; Lawson, J.D.; Askew, T.E.A. Strategic resource development options in England and Wales. *Water Environ. J.* **1996**, *10*, 160–169. [CrossRef]
7. Su, H.B.; Zhang, T.M.; Hu, C.Y.; Long, L.Y. Calculation of ecological compensation for water sources for water diversion projects. *IOP Conf. Ser. Earth Environ. Sci.* **2016**, *39*, 12004. [CrossRef]

8. Yang, G.Q.; Li, Y.; Jiang, Y.H.; Liu, H.Y.; Jin, Y. A discussion of the emergency groundwater supply mode in Ningbo City-Dasong River Basin as an example. *Yangtze River* **2020**, *9*, 1–7.

9. Wu, Z.W.; Li, Z.C.; Wang, H.L. Simulation of seepage field under an emergency condition of groundwater supply at Maanshan City. *J. Water Resour. Archit. Eng.* **2020**, *18*, 244–249.

10. Zhu, H.H.; Dong, Y.N.; Xing, L.T.; Lan, X.X.; Yang, L.Z.; Liu, Z.Z.; Bian, N.F. Protection of the Liuzheng water source: A Karst WATER system in Dawu, Zibo, China. *Water* **2019**, *11*, 698. [CrossRef]

11. Tu, L.Q. Estimate of urban emergency water source in Xincai County. *Ground Water* **2020**, *42*, 91–93.

12. Zhang, Y.; Liu, Y.; Mao, L.; Gong, X.L.; Ye, S.J.; Liu, Y.; LI, J. Risk prediction of groundwater emergency water sources in Nantong Binhai new area. *J. Water Resour. Water Eng.* **2019**, *30*, 100–106.

13. Tu, S.B. Study on groundwater emergency water source in Huadu District, Guangzhou. *Ground Water* **2019**, *41*, 11–13.

14. Sun, Y.; Yue, Y.H.; Liu, Z.G.; Cai, Z.C.; Zheng, T. Evaluation on the groundwater resource in riverside emergency water source based on GMS. *Geol. Resour.* **2019**, *28*, 72–77.

15. De Melo, M.T.C.; Fernandes, J.; Midoes, C.; Amaral, H.; Almeida, C.C.; Da Silva, M.A.M.; Mendonca, J.J. Identification and management of strategic groundwater bodies for emergency situations in Portugal. In Proceedings of the 33rd International Geological Congress, Oslo, Norway, 6–14 August 2008.

16. Michalko, J.; Kordík, J.; Bodiš, D.; Malík, P.; Černák, R.; Bottlik, F.; Veis, P.; Grolmusová, Z. Identification and management of strategic groundwater bodies for emergency situations in Bratislava District, Slovak Republic. In Proceedings of the Biennial Conference of the Ground-Water-Division of the Geological-Society-of-South-Africa, Pretoria, South Africa, 10–12 October 2011; CRC Press: Leiden, The Netherlands, 2014; Volume 19, pp. 165–178.

17. Schwecke, M.; Simons, B.; Maheshwari, B.; Ramsay, G. Integrating alternative water sources in urbanized environments. In Proceedings of the 2nd Conference on Sustainable Irrigation Management, Technologies and Policies, Univ. Alicante, Alicante, Spain, 11–13 June 2008; WIT Press: Southampton, UK, 2008; pp. 351–359.

18. Verjus, P. *Albian-Neocomien Underground Water Resources. How to Safeguard and Manage an Emergency Strategic Resource for Drinking Water*; Societe Hydrotechnique de France: Paris, France, 2003; pp. 51–56.

19. Lowry, T.S.; Bright, J.C.; Close, M.E.; Robb, C.A.; White, P.A.; Cameron, S. Management gaps analysis: A case study of groundwater resource management in New Zealand. *Int. J. Water Resour. Dev.* **2003**, *19*, 579–592. [CrossRef]

20. Merz, C.; Lischeid, G. Multivariate analysis to assess the impact of irrigation on groundwater quality. *Environ. Earth Sci.* **2019**, *78*, 1–11. [CrossRef]

21. Carrillo-Rivera, J.J.; Cardona, A.; Huizar-Alvarez, R.; Graniel, E. Response of the interaction between groundwater and other components of the environment in Mexico. *Environ. Geol.* **2008**, *55*, 303–319. [CrossRef]

22. Wang, S.F.; Li, J.; Liu, Y.Z.; Liu, J.R.; Wang, X. Impact of South to North Water Diversion on groundwater recovery in Beijing. *China Water Resour.* **2019**, *7*, 26–30.

23. Meng, Y.; Zheng, X.; Qi, S.; Mingtang, L.; Zhuojun, L.; Long, J. Safe pumping in areas prone to karst collapses: A case study of the urban emergency water source of the Guanghua basin in the Pearl River Delta. *Carsologica Sin.* **2019**, *38*, 924–929.

24. Amar, P.K. Ensuring safe water in post-chemical, biological, radiological and nuclear emergencies. *J. Pharm. BioAllied Sci.* **2010**, *2*, 253–266. [CrossRef]

25. Lan, Y.; Jin, M.G.; Yan, C.; Zou, Y.Q. Schemes of groundwater exploitation for emergency water supply and their environmental impacts on Jiujiang City, China. *Environ. Earth Sci.* **2015**, *73*, 2365–2376. [CrossRef]

26. Dai, C.L.; Chi, B.M.; Liu, Z.P. City's emergency water source field in north China with the example of Changchun City. *Procedia Environ. Sci.* **2012**, *12*, 474–483. [CrossRef]

27. Zhu, H.H.; Zhou, J.W.; Jia, C.; Yang, S.; Wu, J.; Yang, L.Z.; Wei, Z.R.; Liu, H.W.; Liu, Z.Z. Control effects of hydraulic interception wells on groundwater pollutant transport in the Dawu water source area. *Water* **2019**, *11*, 1663. [CrossRef]

28. Song, P.B.; Wang, C.; Zhang, W.; Liu, W.F.; Sun, J.H.; Wang, X.Y.; Lei, X.H.; Wang, H. Urban multi-source water supply in China: Variation tendency, modeling methods and challenges. *Water* **2020**, *12*, 1199. [CrossRef]

29. Zhang, Y.; Zhang, K.; Niu, Z. Reservoir-Type water source vulnerability assessment: A case study of the Yuqiao Reservoir, China. *Hydrol. Sci. J.* **2016**, *61*, 1291–1300. [CrossRef]

30. Mussá, F.E.F.; Zhou, Y.; Maskey, S.; Masih, I.; Uhlenbrook, S. Groundwater as an emergency source for drought mitigation in the Crocodile River catchment, South Africa. *Hydrol. Earth Syst. Sci.* **2015**, *19*, 1093–1106. [CrossRef]

31. Bozek, F.; Bumbova, A.; Bakos, E.; Bozek, A.; Dvorak, J. Semi-Quantitative risk assessment of groundwater resources for emergency water supply. *J. Risk Res.* **2015**, *18*, 505–520. [CrossRef]

32. Capelli, G.; Salvati, M.; Petitta, M. Strategic groundwater resources in Northern Latium volcanic complexes (Italy): Identification criteria and purposeful management. In Proceedings of the International Symposium on Integrated Water Resources Management, Unvi. Calif, Davis, CA, USA, 21–23 April 2000; IAHS Press: Wallingford, UK, 2001; Volume 272, pp. 411–416.

33. Perfler, R.; Unterwainig, M.; Mayr, E.; Neunteufel, R. The security and quality of drinking water supply in Austria–Factors, present requirements and initiatives. *Österreichische Wasser Abfallwirtsch* **2007**, *59*, 125–130. [CrossRef]

34. Zhang, X.L.; Li, F.; Liu, H.Z. Analysis on the emergency-type groundwater source fields of Qujing City in Yunnan. *Adv. Mater. Res* **2013**, *610–613*, 2653–2657. [CrossRef]

35. Guo, G.X.; Shen, Y.Y.; Zhu, L.; Li, Y.; Xu, L. Evolution of groundwater flow field in Huairou emergency groundwater well field and its surrounding area under impacts of multiple factors. *South North Water Transf. Water Sci. Technol.* **2014**, *12*, 160–164.

36. Wu, B.H.; Zhou, Q.S.; Pan, X.Q.; Lin, D.H. Research of emergency water source area construction and environmental effect evaluation for Shepan Island of Ningbo City. *Water Resour. Prot.* **2017**, *33*, 41–48.

37. Ye, Y.; Xie, X.M.; Chai, F.X.; Zhao, Q.S. Research on groundwater emergency water source field of city. *Water Resour. Power* **2010**, *28*, 47–49.

38. Liu, J.F. Research on Groundwater Emergency Source Field for Drinkingwater in Urban Jilin City. Ph.D. Thesis, Jilin University, Changchun, China, June 2017.

39. Lu, C.J. Resources Evaluation on Groundwater of the Emergency Wellfield in the NORTH Wuqing District of Tianjin. Master's Thesis, China University of Geosciences (Beijing), Beijing, China, June 2017.

40. Wu, X.Y.; Gu, J.H. Advance in research on urban emergency management capability assessment at home and abroad. *J. Nat. Disasters* **2007**, *16*, 109–114.

41. Polomcic, D.; Gligoric, Z.; Bajic, D.; Cvijovic, C. A hybrid model for forecasting groundwater levels based on fuzzy C-mean clustering and singular spectrum analysis. *Water* **2017**, *9*, 541. [CrossRef]

42. Seyam, M.; Alagha, J.S.; Abunama, T.; Mogheir, Y.; Affam, A.C.; Heydari, M.; Ramlawi, K. Investigation of the influence of excess pumping on groundwater salinity in the Gaza Coastal Aquifer (Palestine) using three predicted future scenarios. *Water* **2020**, *12*, 2218. [CrossRef]

43. Zhu, F. Numerical Simulation of Ordovician Karst Water and Analysis of Environmental Effect of Groundwater Exploitation in Xishan, Beijing. Ph.D. Thesis, Capital Normal University, Beijing, China, May 2014.

44. Yu, G.C.; Zhou, Z.Y.; Yang, L.H.; Huang, W.P.; Wang, X.H. Anticipation of environmental effects and delimitation of emergency groundwater sources in Jiaxing. *Bull. Sci. Technol.* **2017**, *33*, 53–57.

45. Zhu, M.J.; Wang, S.Q.; Kong, X.L.; Zheng, W.B.; Feng, W.Z.; Zhang, X.F.; Yuan, R.Q.; Song, X.F.; Sprenger, M. Interaction of surface water and groundwater influenced by groundwater over-extraction, waste water discharge and water transfer in Xiong'an new area, China. *Water* **2019**, *11*, 539. [CrossRef]

46. Liu, S.X.; Shen, H.T.; Zhao, J.K.; Wu, M.J. Geo-Environmental effects since the beginning of groundwater exploitation restriction in the Zhejiang coastal plain. *J. Geol. Hazard Environ. Preserv.* **2013**, *24*, 37–44.

47. Li, C.X.; Chen, Q.Q.; Zhang, J.Q.; Yang, S.Y.; Fan, D.L. Stratigraphy and paleoenvironmental changes in the Yangtze Delta during the Late Quaternary. *J. Asian Earth Sci.* **2000**, *18*, 453–469. [CrossRef]

48. Ma, Q.; Luo, Z.; Howard, K.W.F.; Wang, Q. Evaluation of optimal aquifer yield in Nantong City, China, under land subsidence constraints. *Q. J. Eng. Geol. Hydrogeol.* **2018**, *51*, 124–137. [CrossRef]

49. Diersch, H.-J. *FEFLOW: Finite Element Modeling of Flow, Mass and Heat Transport in Porous and Fractured Media*; Springer: Berlin/Heidelberg, Germany, 2014; p. 996.

50. Huo, Z.L.; Feng, S.Y.; Kang, S.Z.; Cen, S.J.; Ma, Y. Simulation of effects of agricultural activities on groundwater level by combining FEFLOW and GIS. *N. Z. J. Agric. Res.* **2007**, *50*, 839–846. [CrossRef]

51. Xue, Y.Q.; Xie, C.H. *Numerical Simulation for Groundwater*; China Science Publishing & Media Ltd.: Beijing, China, 2007.

52. Chen, X.L. Measurement of streambed hydraulic conductivity and its anisotropy. *Environ. Geol.* **2000**, *39*, 1317–1324. [CrossRef]

53.　Zhu, S.F.; Sheng, J.; He, T.J. The application of geophysical well logging in a hydrogeological survey in the Nantong area. *Shanghai Land Resour.* **2016**, *37*, 89–91.